Localized level hopping transport in La(Sr)CrO_3

D. P. Karim and A. T. Aldred
Argonne National Laboratory, Argonne, Illinois 60439
(Received 26 February 1979)

High-temperature measurements have been performed on the electronically conducting oxide system $La_{1-x}Sr_xCrO_3$ ($0 \leq x \leq 0.4$). The electrical conductivity displayed thermally activated temperature dependence between 300 and 1900 K with activation energies that varied between 0.11 and 0.19 eV. Seebeck coefficients measured over a similar temperature range showed little temperature dependence, an indication that the carrier mobility, rather than the carrier concentration, is thermally activated. The magnetic susceptibility was Curie-Weiss-like between 600 and 1100 K with an effective moment that decreased with an increase in strontium concentration. These results are shown to be consistent with transport by the adiabatic hopping of small polarons.

I. INTRODUCTION

There has been considerable interst in the system $La_{1-x}Sr_xCrO_3$ in the past few years due largely to its very refractory nature (melting point ~2600 K) and its good electrical conductivity over a wide range of temperatures. These properties, and in particular the fact that the conductivity is electronic in nature and only weakly temperature dependent between room temperature and ~2000 K, make La(Sr)CrO_3 attractive as a potential material for the construction of electrodes for magnetohydrodynamic generators.[1]

Pure $LaCrO_3$ has a slightly distorted pseudocubic perovskite structure (Fig. 1) that undergoes a symmetry chage from orthorhombic at low temperatures to rhombohedral above 560 K.[2] The substitution of Sr for La has been shown to lower this transition temperature (to 190 K at $x = 0.16$).[3]

Both pure and Sr-doped $LaCrO_3$ exhibit thermally activated conductivity behavior with the doped material having a smaller activation energy and a larger pre-exponential factor in the conductivity. Thermally activated conductivity can arise from quite different microscopic charge transport mechanisms. For instance, the number of carriers involved in conduction can be thermally activated as in broad-band semiconductors, where carriers are excited into nonlocalized states in a conduction or valence band, or in disordered systems where carriers are excited from localized states into extended states above a mobility gap. In these cases, the mobility generally exhibits a simple power-law temperature dependence, where the power is determined by the predominant scattering mechanism. Thermally activated conductivity can also occur in systems where the number of carriers is constant or slowly varying, but where the mobility is exponentially dependent on temperature. Such is the case where transport is via the hopping motion of spatially localized charge carriers. The localization can result from the absence of any long-range order (Anderson localization[4]), or from lattice-distortion localization due to a strong electron-phonon interaction, i.e., small-polaron formation. It is small-polaron hopping transport which, we believe, occurs in $La_{1-x}Sr_xCrO_3$.

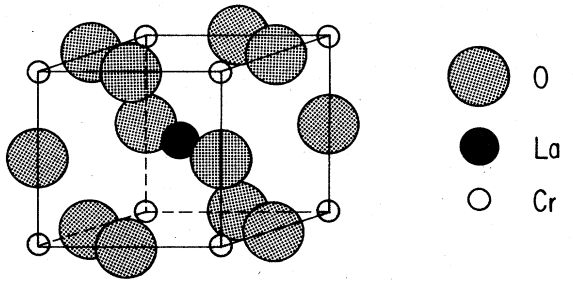

FIG. 1. Cubic perovskite unit cell.

The conditions for small-polaron formation are a narrow conduction band and a large electron-phonon interaction[5–7] which allow a charge carrier to locally distort the lattice around it and subsequently become "self-trapped" in the resulting potential well. The carrier, together with the distortion field, then move by activated hopping.

In $La_{1-x}Sr_xCrO_3$, Sr^{2+} ions are distributed randomly on La^{3+} lattice sites. It is generally believed that charge compensation takes place via the chromium ions ($Cr^{3+} \rightarrow Cr^{4+}$) giving a *d*-band, *p*-type conductivity, although charge compensation could also take place, in principle, by the creation of oxygen vacancies.

We have undertaken a series of dc electrical conductivity, Seebeck effect, and magnetic susceptibility measurements on $La_{1-x}Sr_xCrO_3$ ($0 \leq x \leq 0.4$) over the range 300–1900 K with the purpose of elucidating the nature of the carriers and the transport mechanism.

II. EXPERIMENTAL

The samples used in this study were obtained from Dr. Harlan U. Anderson of the University of Missouri at Rolla. The preparation technique has been described in detail elsewhere.[8–10] Briefly, the procedure involves mixing and firing organic precursors to yield a fine-grained, compositionally homogeneous powder. The powder is then pressed into disks and sintered at 1970 K in an oxygen partial pressure, P_{O_2}, of 10^{-12} atm. The low P_{O_2} increases the sintered density, apparently by inhibiting the oxidation of the chromic ion to oxidation states with more volatile oxides.[9,11] The disks were subsequently annealed in pure oxygen at 1700 K to restore oxygen lost in the sintering process. Fracture surfaces of several of the samples were examined with a scanning electron microscope equipped with energy dispersive x-ray analysis to construct fluorescent x-ray elemental maps of the surfaces. The elemental maps showed uniform distributions of Cr, La, and Sr within the samples to a resolution of ~ 1 μm. This is consistent with x-ray results[12] which show that the $La_{1-x}Sr_xCrO_3$ system forms a single phase at least out to $x = 0.35$.

Electrical conductivities were measured by a normal four-probe quasi-dc method to overcome any effects of barrier layers or nonohmic contacts. The samples were bar-shaped with typical dimensions $15 \times 2 \times 2$ mm^3. Pressure contacts and all lead-ins were made from platinum, and a type-S (Pt vs Pt–10-at.%-Rh) thermocouple was used for temperature measurement. Controlled ambient conditions were obtained in an Astro model 1000 A furnace (300–2000 K) equipped with an alumina muffle tube. Different oxygen partial pressures were produced by a controlled flowing atmosphere of O_2-Ar ($P_{O_2} = 1 - 10^{-4}$ atm) or CO-CO_2 ($P_{O_2} < 10^{-6}$ atm).

Seebeck-voltage measurements were made below 500 K on samples placed between two blocks machined of OFHC (oxygen-free high-conductivity) copper. A copper wire was bonded to the back side of each block, and an insulated constantan wire was led into the block through a small axial hole and bonded at the center of the block face in contact with the sample (Fig. 2). The high thermal conductivity of the copper blocks helped to minimize radial temperature gradients. The blocks were fitted into teflon holders, and manganin-wound heaters were wrapped around the teflon near the ends and in contact with the copper blocks in order to produce the temperature gradient. The holders were spring loaded together to provide contact pressure between the sample and the copper blocks, and the assembly was placed inside a thin-walled stainless-steel can. The can was then placed inside a controlled-ambient furnace.

Measurements were carried out using an instrumentation amplifier–analog subtraction circuit based on a design by Ecklund and Mabatah.[13] Briefly, the circuit is comprised of two gain- and bandwidth-matched amplifiers A_1 and A_2. The inputs to the two amplifiers were the two copper leads and two constantan leads, respectively. The outputs from A_1 and A_2 were inputs to a third differential amplifier A_3. The outputs of A_3 and A_1 are fed to the X and Y axes of a plotter, respectively. As explained in Ref. 13, when a small time-dependent temperature gradient is applied across the sample, a straight line is plotted whose slope can be used to determine the Seebeck coefficient of the sample. In our measurements, the heater was used to supply a temperature gradient which grew to ~ 2 K in one minute. When the heater was turned off, the straight lines produced on heating were retraced as the thermal gradient relaxed back to zero.

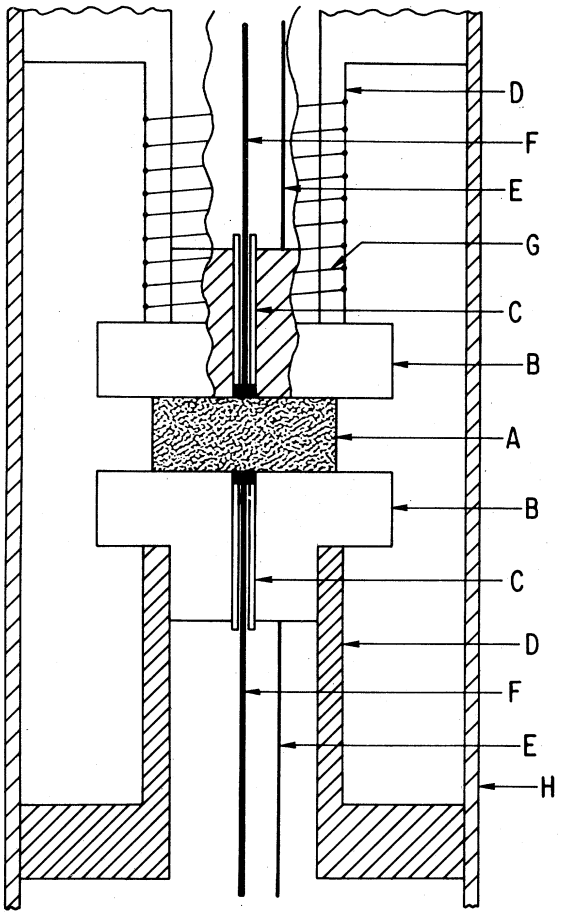

FIG. 2. Schematic of the lower-temperature Seebeck apparatus. A, sample; B, copper block, C, insulator; D, teflon block holder; E, copper thermocouple lead; F, constantan thermocouple lead; G, manganin heater; H, stainless-steel can.

For Seebeck measurements between 500 and 1500 K, blocks similar to the copper blocks (Fig. 2) were

machined from 99.99+% platinum and used in a configuration similar to that presented by Ruka *et al.*[14] Thermocouple junctions were made with Pt–10-at.%-Rh wire inserted through an axial hole in the block and insulated from the block, except at the junction itself, by alumina tubing. The junction was formed by creating a slightly oversized bead on the Pt–10-at.%-Rh wire and forcing the bead into the axial hole. A Pt–10-at.%-Rh wire heater wound on an alumina holder generated the time-dependent temperature gradients. The assembly was placed inside the Astro furnace employed for the conductivity measurements. The same analog subtraction circuit described previously was used. The sensitivity of the type-*S* system is substantially lower than that of copper-constantan and becomes quite temperature dependent below ~500 K. Good thermal contact was also more of a problem with the high-temperature system where a simple ceramic weight was used to press the blocks and sample together. Inadequate thermal contact produced some curvature in the lines on the *X-Y* plotter. The curvature could be minimized by applying the time-dependent thermal gradient more slowly. The samples generally stuck to the platinum blocks after measurements and could not be recovered without breaking. Consequently, the samples used for the copper block system (which was put together after the higher-temperature data were taken) were from the same batch but were not identical samples used in taking the higher-temperature data.

The magnetic susceptibility measurements were performed by the Faraday method over the range 300–1100 K on a system that included a Varian electromagnet equipped with constant-gradient polecaps, an Ainsworth electrobalance, and a sheathed nichrome heating element. The sample was hung from the balance by a suspension consisting of a tantalum chain, a quartz fiber in the region of large thermal and magnetic field gradients, and a tantalum sample holder. Temperatures were measured with a type-*S* thermocouple located adjacent to the sample. To take account of possible temperature differences between the sample and the thermocouple, the thermocouple was calibrated in a separate experiment in which a second type-*S* thermocouple was placed on the suspension in direct contact with the sample holder. The susceptibility measurements were carried out in an ambient vacuum of $\sim 10^{-6}$ Torr, and all the samples showed some weight loss (<1%) over the entire temperature run, presumably resulting from loss of oxygen.

III. RESULTS

The electrical conductivity σ was measured as a function of temperature for several $La_{1-x}Sr_xCrO_3$ samples in the composition range $x = 0$–0.4. Measurements were performed from 300 to 1770 K on all samples, and on some data were taken as high as 1970 K. However, extra care was taken not to prolong measurements above 1900 K because drifts in the conductivity of ~2–3% were observed over several hours, possibly due to further sintering.

Figure 3 is a plot of $\log_{10}$ conductivity versus inverse temperature for several dopant concentrations; note that the data shows considerable curvature when plotted in this manner. Figure 4 shows the same data replotted in the form $\log(\sigma T)$ vs T^{-1}. For the most part, the conductivity is well represented by the function form $\sigma \propto (1/T)\exp(E/kT)$. In Sec. IV we will discuss why this form is consistent with small-polaron hopping transport. The activation energy obtained by fitting the data in this way is 0.192 eV for pure $LaCrO_3$. The Sr-doped samples show decreased activation energies at higher-Sr concentrations. If the number of charge carriers scales with the Sr doping level, we would expect the high-temperature conductivity to scale also. Figure 5 shows the conductivity at 1500 K

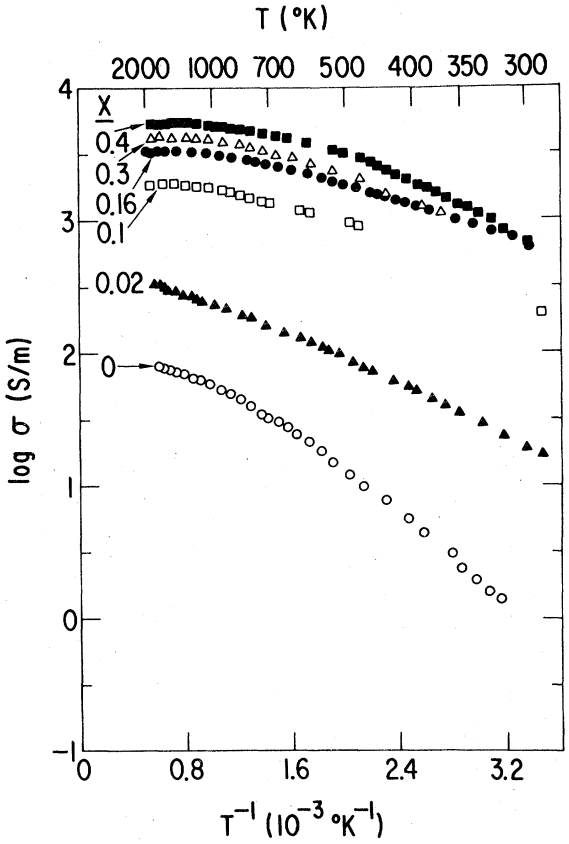

FIG. 3. $\text{Log}_{10}\sigma$ vs T^{-1} for $La_{1-x}Sr_xCrO_3$ samples with $x = 0.0$, 0.02, 0.1, 0.16, 0.3, and 0.4 at $P_{O_2} = 1$ atm. The Systéme Internationale unit of conductivity the siemens (S), is numerically equal to 1 mho.

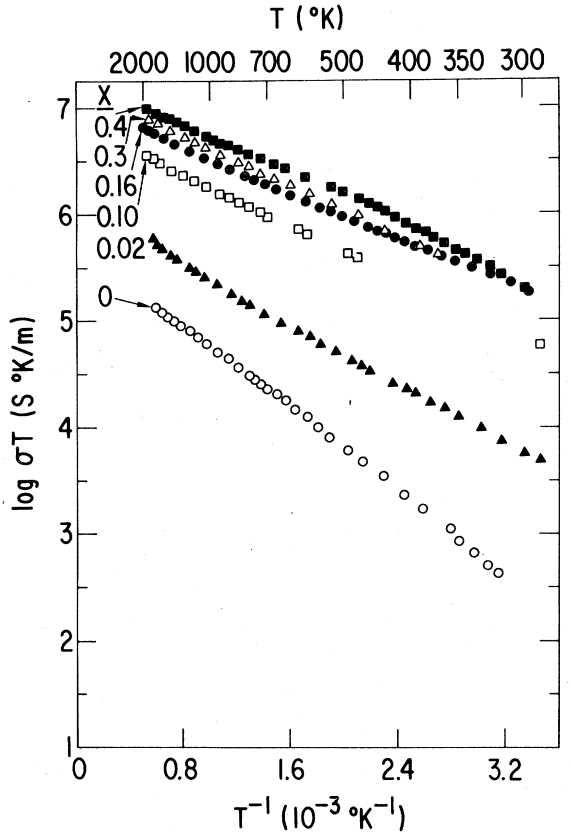

FIG. 4. Data of Fig. 3 replotted as $\log_{10}\sigma T$ vs T^{-1}.

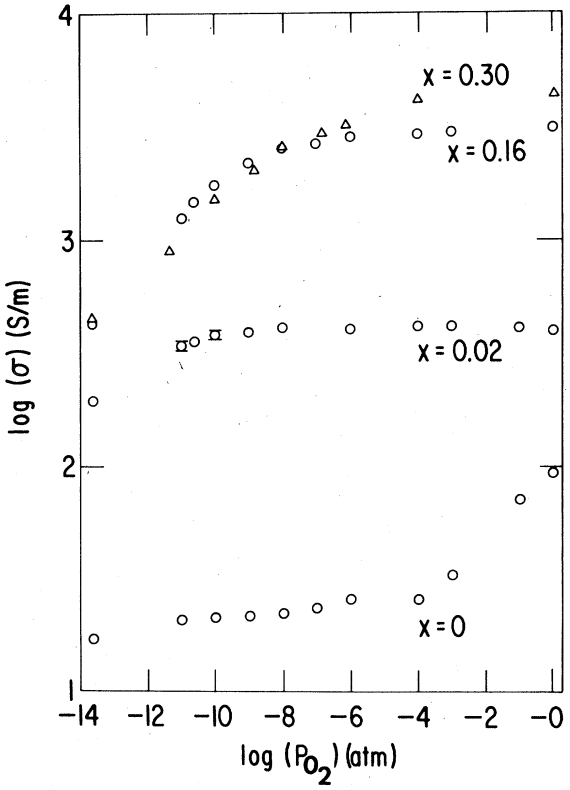

FIG. 6. Oxygen partial pressure dependence of the conductivity of $La_{1-x}Sr_xCrO_3$ at $T=1675$ K for $x=0.0$, 0.2, 0.16, and 0.30. For familiarity, the pressures are given in atmospheres, 1 atm $\equiv 1.013\times10^5$ pascals.

plotted as a function of sample composition. The conductivity is initially proportional to Sr concentration and levels off moderately at higher values.

Figure 6 shows the variation of conductivity with oxygen partial pressure for four samples at 1670 K. In pure $LaCrO_3$ there is an initial drop in conductivity

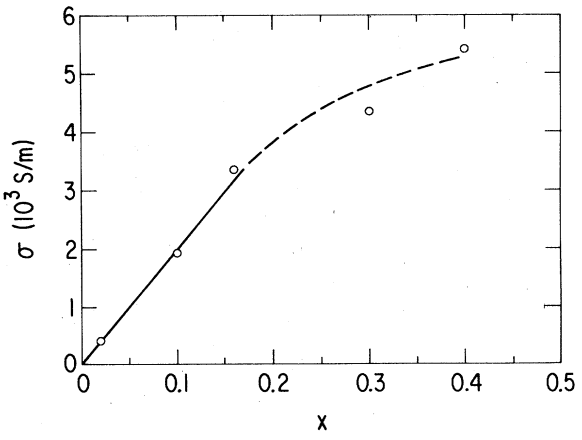

FIG. 5. Compositional dependence of the conductivity of $La_{1-x}Sr_xCrO_3$ at $T=1500$ K and $P_{O_2}=1$ atm.

with a decrease in P_{O_2} followed by a leveling-off region. The drop is an indication that removal of oxygen from the system decreases the number of carriers predominantly responsible for the conductivity. The Sr-doped samples show very little change in conductivity until P_{O_2} is decreased to much lower values. This is easily understood inasmuch as the carrier concentrations introduced by doping will be much larger than the changes in the carrier concentration produced by modest variation in P_{O_2}. However, it is somewhat surprising that the more heavily doped samples show a greater drop in conductivity at low P_{O_2} than the $x=0.02$ sample. Such an effect could be explained if, due perhaps to structural considerations, there was a greater tendency toward charge compensation by oxygen vacancy creation rather than by Cr^{4+} creation in the more heavily Sr-doped samples. A more detailed study of the temperature and P_{O_2} dependence of the conductivity in $LaCrO_3$ yielded the results shown in Fig. 7.

Thermoelectric measurements were carried out to obtain information on the density and sign of the charge carriers. Figure 8 shows measured values of

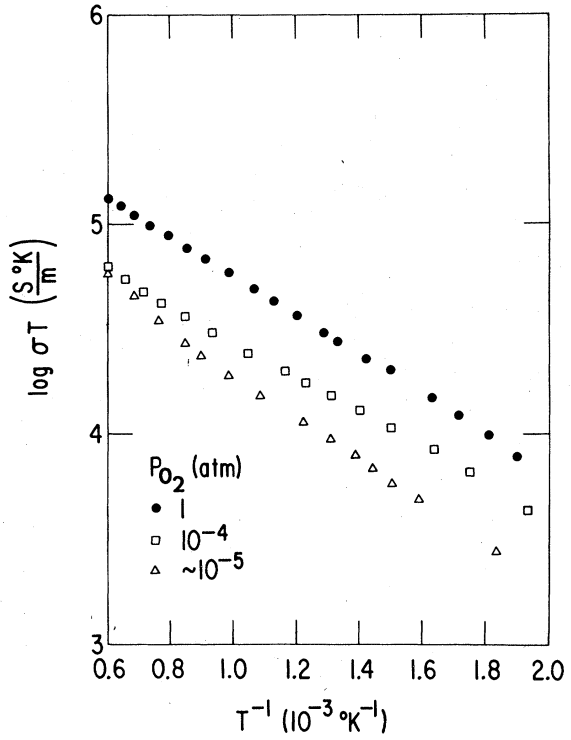

FIG. 7. $\text{Log}_{10}\sigma T$ vs T^{-1} for $LaCrO_3$ equilibrated in different oxygen partial pressures.

the Seebeck coefficient as a function of temperature for several samples which were equilibrated in pure oxygen at high temperature. The positive sign of the Seebeck coefficient indicates that p-type conductivity dominates in both doped and undoped samples. The Sr-doped samples show an essentially temperature-independent Seebeck coefficient over a very broad temperature range. This result implies that the number of charge carriers does not vary with temperature and depends only on the doping level. The thermopower of pure $LaCrO_3$ is greater overall and increases in value at lower temperatures. The data taken with the copper blocks ($T < 500$ K) showed considerably less scatter and better reproducibility than the high-temperature data taken with the platinum block system.

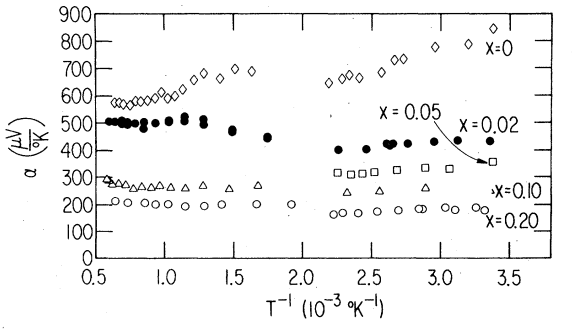

FIG. 8. Seebeck coefficient vs T^{-1} for $La_{1-x}Sr_xCrO_3$ samples with $x = 0.0$, 0.02, 0.05, 0.10, and 0.20 at $P_{O_2} = 1$ atm. Data for $T^{-1} < 2.0$ were taken with the platinum block system, and data for $T^{-1} > 2.0$ were taken with the copper block system.

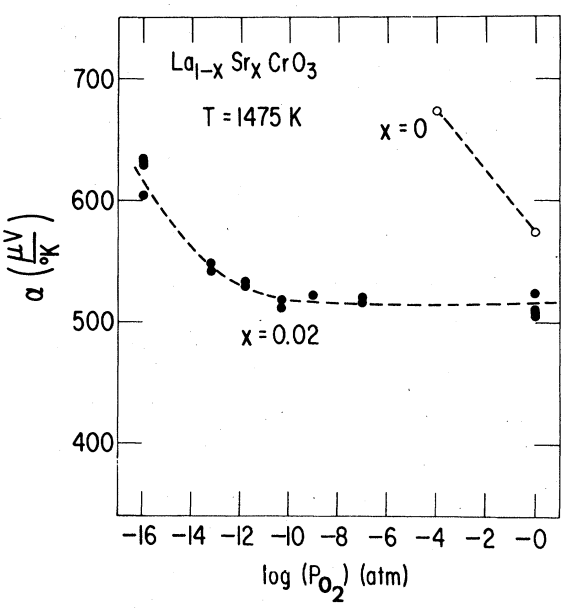

FIG. 9. Oxygen partial pressure dependence of the Seebeck coefficient of $LaCrO_3$ and $La_{0.98}Sr_{0.02}CrO_3$.

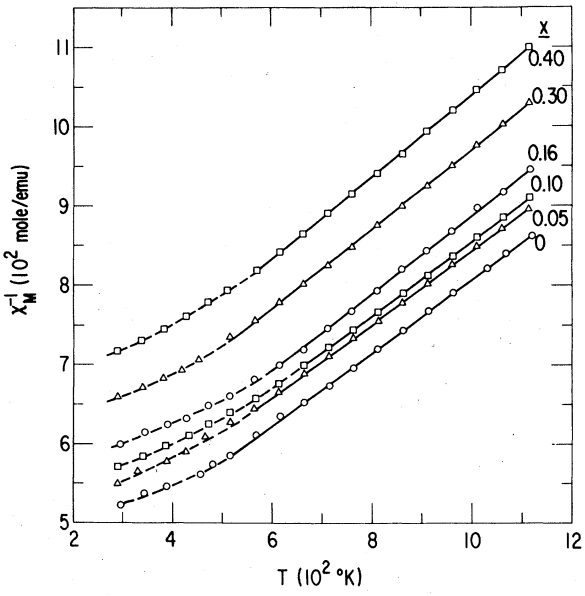

FIG. 10. Inverse magnetic susceptibility vs temperature for $La_{1-x}Sr_xCrO_3$ samples with $x = 0.0$, 0.05, 0.10, 0.16, 0.30, and 0.40.

TABLE I. Curie-Weiss parameters of $La_{1-x}Sr_xCrO_3$ samples.

x	C (emu/mole °K)	μ_{eff} (μ_B/mole)	Θ (°K)
0	2.18(2)[a]	4.19(3)	−759(12)
0.05	2.14(1)	4.15(2)	−802(7)
0.10	2.13(1)	4.15(2)	−821(10)
0.16	2.07(2)	4.09(5)	−836(19)
0.30	2.00(1)	4.02(3)	−944(15)
0.40	1.95(2)	3.96(3)	−1023(12)

[a]Numbers in parentheses denote statistical uncertainties as given by the least-squares analysis.

The P_{O_2} dependence of the high-temperature Seebeck coefficients for two different sample compositions is shown in Fig. 9. The $x=0.02$ sample shows little, if any, variation in α until P_{O_2} drops below about 10^{-12} atm. The pure $LaCrO_3$ sample on the other hand, shows a significant increase (~100 μV/°K) in the Seebeck coefficient between $P_{O_2}=1$ atm and 10^{-4} atm. Data taken on the pure sample for $P_{O_2}<10^{-4}$ atm were erratic and led to irreproducible results upon subsequent re-equilibration in oxygen.

The magnetic susceptibility χ of each sample was found to be independent of magnetic field over the entire range of field (2–11 kOe) and temperature (300–1100 K). The inverse molar susceptibility values are shown as a function of temperature in Fig. 10. The monotonic decrease in susceptibility with an increase in Sr concentration is evident. Above 600 K, the data are accurately represented by the Curie-Weiss law,

$$\chi=\frac{C}{T-\Theta}\ , \tag{1}$$

and the solid lines through the data represent the results of least-squares fit to Eq. (1). The parameters obtained are listed in Table I.

IV. DISCUSSION

A semiempirical model has been put forward by Goodenough[15,16] to explain the overall electronic properties of transition-metal oxides and perovskite-structure mixed oxides. According to the model, the degree of localization of the transition-metal d electrons depends on the overlap integrals with d states on neighboring transition-metal cations. Consider the (pseudo-) cubic perovskite (ABO_3) cell in Fig. 1. In the case of $LaCrO_3$, chromium atoms sit on the cube corners (B sites) with lanthanum atoms at the body-center position (A sites) and oxygen atoms on the edge centers. It is believed that the chromium d states with t_{2g} symmetry have small overlap integrals resulting in narrow bands and a tendency toward localization, whereas d states with e_g symmetry have larger overlap, due to hybridization with oxygen p_σ levels, and form a wider band of itinerant states higher in energy and not occupied in the ground state of the system. All levels associated with the A sublattice atoms are well above or below the Fermi energy, and their primary role is to determine the occupancy of the t_{2g} chromium states through charge compensation. Replacement of a La^{3+} ion with a Sr^{2+} ion on an A site will create a hole in the Cr t_{2g} band.

A small polaron will be formed if the effective mass of the rigid lattice hole is large enough and coupling to optical phonons is strong. The hole becomes trapped in the potential well created by the distortion of the surrounding lattice and the lattice relaxation will narrow the band even further.[5] The polaron can hop to a neighboring site when the thermal fluctuations reduce the depth of the potential well and create an empty well at a neighboring lattice site. At this point we consider two cases.

(a) If, during the period when an electron sees an exicted lattice state (on the order of $1/\nu_0$, where ν_0 is an optical-phonon frequency), it can tunnel between the potential wells several times, the mobility, μ, is of the form

$$\mu=(1-x)\frac{ea^2\nu_0}{kT}\exp\left(-\frac{W_H}{kT}\right)\ , \tag{2}$$

where x is the fraction of occupied sites, e is the charge of the carriers, a is the intersite distance, k is Boltzmann's constant, and W_H is a hopping energy. This is known as the "adiabatic" case.

(b) In the nonadiabatic case, small wave-function overlaps between states on neighboring sites result in a tunneling probability[5]

$$P=\frac{J^2}{2\hbar}\left(\frac{\pi}{W_H kT}\right)^{1/2}\ll 1 \tag{3}$$

and mobility

$$\mu=(1-x)\frac{ea^2}{kT}P\exp\left(-\frac{W_H}{kT}\right)\ , \tag{4}$$

where J is half the rigid-lattice bandwidth. Note that in the nonadiabatic case there is an extra factor of $T^{-1/2}$ outside the exponential.

Inasmuch as the experimentally measured conductivity yields the product of mobility and carrier concentration, we would like an independent determination of the carrier concentration such as can be obtained from thermoelectric data. In the literature concerning thermoelectric effects in the small-polaron hopping regime, much use has been made of the

"Heikes formula"[17] for the Seebeck coefficient

$$\alpha = \pm \frac{k}{e}\left[\ln\left(\frac{1-x}{x}\right) + \frac{\Delta S^1}{k}\right] , \tag{5}$$

where x is the fraction of hopping sites which are occupied and ΔS^1 is the entropy associated with the ionic relaxation around the polaron. The sign of the Seebeck coefficient is the same as the sign of the carriers. It has been point out[18,19] that the inclusion of spin degeneracy changes the form to

$$\alpha = \pm \frac{k}{e}\left\{\ln\left[2\left(\frac{1-x}{x}\right)\right] + \frac{\Delta S^1}{k}\right\} . \tag{6}$$

Austin and Mott[20] estimate the term $\Delta S^1/k$ to be $-0.1-0.2$. In any case, small-polaron hopping should lead to a temperature-independent Seebeck coefficient whose magnitude is primarily dependent on the density of carriers. This is to be contrasted with the expression for the Seebeck coefficient of a broad-band semiconductor where transport is by thermal activation of carriers into a conduction or valence band,[21] i.e.,

$$\alpha = \pm \frac{k}{e}\left(\frac{\Delta E}{kT} + \frac{5}{2} + r\right) , \tag{7}$$

where ΔE is the energy between the Fermi level and the band involved in transport, and r is a constant which depends on the dominant scattering mechanism.

Our results support the case for transport in $La_{1-x}Sr_xCrO_3$ by thermally activated hopping between localized hole states on the chromium sublattice. In all of the Sr-doped samples the Seebeck coefficient is essentially temperature independent. This is the expected result for the hopping model with a fixed number of carriers. The band model yields [Eq. (7)] the temperature-dependent term $(k/e)(\Delta E/kT)$. If ΔE is associated with the measured activation energy for conduction, a component of the Seebeck coefficient that is linear in $1/T$ and varies by -350 μV/°K over the temperature range of the measurements is obtained. This result is in clear contradition to the experimentally measured temperature dependence for the doped samples (Fig. 8). If we assume that one charge carrier is created for each Sr atom substituted into $LaCrO_3$ we can compare the Seebeck results more quantitatively with the Heikes formula modified to include spin degeneracy [Eq. (6)]. The results are given in Table II. Despite the neglect of the $\Delta S^1/k$ term in Eq. (6) and carrier interaction effects, the overall agreement between $\ln 2[(1-x)/x]$ and $e\alpha/k$ is reasonably good. Additionally, the scaling of the carrier concentration with Sr addition at lower doping concentration is supported by the high-temperature conductivity results (Fig. 5).

TABLE II. Seebeck-coefficient results for $La_{1-x}Sr_xCrO_3$ samples. Mean values for α between 300 and 450 K are reported.

x	$\alpha\left(\frac{\mu V}{K}\right)$	$\ln 2\left(\frac{1-x}{x}\right)$	$\frac{e}{k}\alpha$
0.02	423	4.58	4.91
0.05	328	3.64	3.81
0.10	251	2.89	2.91
0.20	179	2.08	2.08

If the carrier concentration is indeed temperature independent, we may interpret the activation energy for conduction as the mobility activation energy. The values of the activation energy determined from the data depend on the temperature dependence of the pre-exponential term used. As stated previously, the form $\mu = (C'/T)e^{-E/kT}$, expected for adiabatic hopping mobility, fits the data quite well, and the parameters obtained are given in Table III. The decrease in the activation energy with an increase in carrier concen-

TABLE III. Parameters obtained by fitting conductivity data for $La_{1-x}Sr_xCrO_3$ samples to an equation of the form $\sigma = (C/T)\exp(-E/kT)$.

x	E (eV)	$C\left(10^7 \frac{S\ °K}{m}\right)$	$C' = \frac{C}{N}\left(10^{-3}\frac{m^2\ °K}{V\ sec}\right)$	ν_0 (10^{13} Hz)
0	0.192	0.052	...	...
0.02	0.134	0.111	2.04	1.19
0.10	0.120	0.741	2.72	1.73
0.16	0.102	1.06	2.44	1.66
0.30	0.115	1.57	1.92	1.57
0.40	0.113	1.95	1.79	1.71

tration is also consistent with small-polaron theory. Mott[22] showed that as polarons approach each other and their polarization clouds start to overlap, the energy required for hopping will be reduced.

The magnitude, as well as the temperature dependence, of the mobility in the doped samples is consistent with the adiabatic hopping of small polarons. If the measured mobility values are substituted in Eq. (2), the optical phonon frequencies ν_0 shown in the last column of Table III are obtained. These values are reasonable for optical phonons in oxides.

The nature of the carriers in nominally pure $LaCrO_3$ is more uncertain. Most probably, there is more than one species of carriers contributing to the measured transport properties. Webb *et al.*[23] assumed that inherent structural defects led to the formation of Cr^{4+} carriers identical to those created by Sr doping. At higher temperatures, mobile oxygen vacancies will also act as *p*-type carriers. Even when they are not mobile, oxygen vacancies will enter the charge balance relations by presenting a charge compensation mechanism that is alternative to Cr^{4+} creation. Contributions to the conductivity from different carriers will presumably be additive. The general expression for the Seebeck effect in this case is

$$\alpha = \frac{1}{\sigma_T} \sum_i \alpha_i \sigma_i \ , \tag{8}$$

where i is an index representing the different carrier species and σ_T is the total conductivity.

The initial drop in the conductivity of $LaCrO_3$ as P_{O_2} is decreased (Fig. 6) can be understood to indicate a reduction in the number of mobile species as oxygen vacancies are introduced. This is confirmed by the P_{O_2} dependence of the Seebeck coefficient at high temperatures (Fig. 9). In $La_{0.98}Sr_{0.02}CrO_3$ the conductivity and Seebeck coefficient are roughly constant down to $P_{O_2} = 10^{-12}$ atm and then begin to vary. This result implies that these low partial pressures are required to introduce vacancy concentra tions of the same magnitude as the doping concentration.

The temperature dependence of the magnetic susceptibility of $LaCrO_3$ above 600 K (Fig. 10) yields an effective magnetic moment (Table I) in good agreement with a value obtained in earlier measurements between 500 and 800 K by Smolenskii *et al.*[24] However, the two curves are displaced from one another by about 5% or ~100 K as reflected by differences in the θ values. The change in slope of the χ^{-1} vs T plot below 600 K (Fig. 10) is qualitatively similar to the behavior found previously.[24] Additional measurements below room temperature, not reported here, show a sharp susceptibility maximum in $LaCrO_3$ at 286 K indicative of the antiferromagnetic ordering reported by Koehler and Wollan.[25] However, Koehler and Wollan quote a Néel temperature of 320 K, and Smolenskii *et al.*[24] find a susceptibility maximum at 271 K. The variations in Néel temperature are probably associated with differences in stoichiometry among the various samples.

The paramagnetic effective moment obtained for $LaCrO_3$ above 600 K (4.19 μ_B/Cr atom, Table I) is in reasonable agreement with the anticipated spin-only moment of 3.87 μ_B/Cr atom $\{=g[S(S+1)]^{1/2}\}$ for the Cr^{3+}, d^3, $S=\frac{3}{2}$ ion. If the effect of introducing Sr^{2+} ions into the lattice is to produce a corresponding number of Cr^{4+} ions $\{g[S(S+1)]^{1/2}=2.83\ \mu_B/\text{Cr atom}\}$, as previously postulated, we would anticipate a decrease in the average effective moment with an increase in the strontium concentration. Such an effect is experimentally observed (Table I and Fig. 11). To provide a more quantitative test, the relative change in effective moment predicted, with a spin-only moment, for the formation of Cr^{4+} ions as the strontium concentration increases has been normalized to the experimentally observed effective moment in pure $LaCrO_3$ and this is shown as the solid line in the lower part of Fig. 11. The experimentally observed change in effective moment with strontium concentration is about a factor of 2 smaller than predicted. Nevertheless, our results give a clear indication of the systematic decrease in susceptibility per mole (or per chromium atom) and a small decrease in the effective moment with an increase in strontium concentration and, thus, are consistent with the model proposed to explain the transport properties of $La_{1-x}Sr_xCrO_3$.

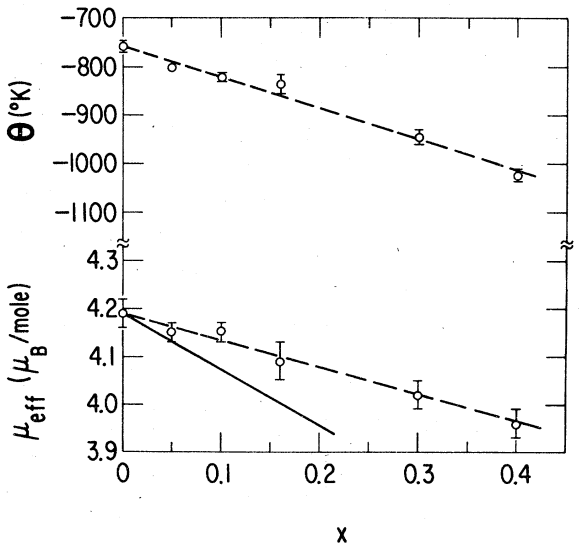

FIG. 11. Curie-Weiss Θ and effective moment, μ_{eff}, vs x in $La_{1-x}Sr_xCrO_3$.

IV. CONCLUSIONS

Measurements of the dc conductivity, Seebeck effect, and magnetic susceptibility have been made on the perovskite-structure system $La_{1-x}Sr_xCrO_3$. The thermally activated behavior of the conductivity, together with an essentially temperature-independent Seebeck coefficient, indicate that transport occurs by hopping between localized levels. The magnitude and temperature dependence of the mobility as inferred from these measurements are consistent with adiabatic small-polaron formation. The Curie-Weiss behavior of the magnetic susceptibility supports this picture and suggests that the levels are associated with the chromium $3d$ band.

ACKNOWLEDGMENTS

This work was supported by the U. S. DOE. We wish to thank Dr. H. U. Anderson of the University of Missouri at Rolla for preparing the samples used in this study and Dr. J. Faber, Dr. J. W. Hafstrom, and Dr. B. W. Veal for helpful discussions.

[1]D. B. Meadowcroft, Br. J. Appl. Phys. 2, 1225 (1969).
[2]J. S. Ruiz, A. M. Anthony, and M. Foex, C. R. Acad. Sci. Ser. B 264, 1271 (1967).
[3]J. Faber, Jr., M. H. Mueller, W. L. Procarione, A. T. Aldred, H. W. Knott, and H. U. Anderson, ANL Report No. ANL-77-21, 156 (1977) (unpublished).
[4]P. W. Anderson, Phys. Rev. 109, 1492 (1958).
[5]T. Holstein, Ann. Phys. (N.Y.) 8, 343 (1959).
[6]J. Appel, Solid State Phys. 21, 193 (1969).
[7]H. Böttger and V. V. Bryksin, Phys. Status Solidi B 78, 9 (1976).
[8]H. U. Anderson, P. Murphy, S. Semachaibovorn, B. Rossing, A. T. Aldred, W. L. Procarione, and R. J. Ackermann, ANL Report No. ANL-77-21, 142 (1977) (unpublished).
[9]L. Groupp, Masters thesis (University of Missouri-Rolla, 1975) (unpublished).
[10]M. Pechini, U. S. Patent 3,330,697, July 11, 1967.
[11]J. W. Halloran and H. U. Anderson, J. Am. Cer. Soc. 57, 150 (1974).
[12]C. P. Khattak and D. E. Cox, Mater. Res. Bull. 12, 463 (1977).
[13]P. C. Ecklund and A. K. Mabatah, Rev. Sci. Instrum. 48, 775 (1977).
[14]R. J. Ruka, J. W. Baverle, and L. Dykstra, J. Electrochem. Soc. 115, 497 (1968).
[15]J. B. Goodenough, J. Appl. Phys. 37, 1415 (1966).
[16]J. B. Goodenough, Phys. Rev. 164, 785 (1967).
[17]R. R. Heikes, in *Thermoelectricity,* edited by R. Heikes and R. Ure (Interscience, New York, 1961), Chap. 4.
[18]A. J. Bosman and H. J. van Daal, Adv. Phys. 19, 1 (1970).
[19]P. M. Chaikin and G. Beni, Phys. Rev. B 13, 647 (1976).
[20]I. G. Austin and N. F. Mott, Adv. Phys. 18, 41 (1969).
[21]N. F. Mott and E. A. Davis, *Electronic Processes in Noncrystalline Materials* (Clarendon, Oxford, 1971).
[22]N. F. Mott, J. Non-Cryst. Solids 1, 1 (1968).
[23]J. B. Webb, M. Sayer, and A. Mansingh, Can. J. Phys. 55, 1725 (1977).
[24]G. A. Smolenskii, V. M. Yudin, E. S. Sher, and Y. E. Stolypin, Sov. Phys. JETP 16, 622 (1963).
[25]W. C. Koehler and E. O. Wollan, J. Phys. Chem. Solids 2, 100 (1957).